REUCP, Petrópolis, Volume 15, n° 1 (2021), P. 36-56
ISSN 2318-0692

DYNAMIC MODELING OF THIN-WALLED SLENDER COLUMNS BRACED BY LINTELS IN SYSTEMS Z AND X: A THEORETICAL AND NUMERICAL APPROACH BY THE CONTINUOUS MEDIUM TECHNIQUE

Weslley I. G. de Melo[1*], Pedro V. C. A. Luz[2] e Normando P. Barbosa[3]

[1]*Universidade Federal Rural de Pernambuco, Recife, 52171-900, PE, Brasil*

[2]*Unidade Acadêmica do Cabo de Santo Agostinho (UACSA) da Universidade Federal Rural de Pernanbuco, Cabo de Santo Agostinho, 54518-430, PE, Brazil*

[3]*Universidade Federal da Paraíba, João Pessoa, 58051-900, PE, Brasil*

Keywords: Thin-walled slender columns, Bracing by lintels in Z and X, Continuous Medium Technique (CMT), Dynamic analysis, Modes of vibration.

Abstract. The thin-walled slender columns are significantly stressed by flexion-torsion, mainly to overcome deep valleys, as is the example of bridge columns, which makes the action of the wind very relevant and, consequently, the analysis of the bracing system. Thus, in resistance to wind action, lintels arranged in Z and X were used. For this purpose, the Continuous Medium Technique (CMT) is used with emphasis on the Wall Panel Theory (WPT). It is worth mentioning that the validation of the theoretical approach via CMT is carried out by numerical simulation in FEM through ANSYS Release 11. With an average accuracy of CMT in the order of 95.85 % for Z lintels, while in X-Bracing, 94.71 % accuracy in the first three modes of vibration.

E-mail addresses: weslley.gomes@ufrpe.br*, pedro200298@hotmail.com, nperazzob@yahoo.com.br.

1 INTRODUCTION

Currently, the modal analysis of structural cores is processed, in the vast majority, in structural calculation offices, using commercial software based on finite element discretization. This leads to blind dimensioning, without the critical view of the engineer over all the stages of the analysis carried out. Thus, it is planned to provide in this article, a mechanism to verify the results obtained by numerical simulations in the mentioned commercial software. More specifically, at the end of this article, a routine of easy attainment of the first modes of vibration for columns in thin-walled cross-sections in C format will be delivered as a result, enabling bracing by lintels under configuration by arrangement in Z or X.

The analytical modeling of bracing lintels, via CMT, starts from the formulation of the equations of stress balance for the bar finite element that was formulated by George Alfred Maney in 1915, see Maney [13]. It turns out that initially, the purpose was the structural analysis of flat frames, which was applied by Goldberg [5] to compute the action of the wind, also in flat frames. Finally, in MacLeod [11] we can see the application of Maney's Equations to extend them to the structural cores.

In more current times, such employment is found in Varjú & Prokié [29] and Melo & Barbosa [17], for the bracing of structural cores braced by horizontal lintels, and under uniform distribution along the height of the column. However, in the case of bridge columns, whether metal or reinforced concrete, it turns out interesting to impose diagonal locks on the open face of the structural core, thus characterizing the need for Z-Bracing.

It is in this sense that the studies by Ricaldoni [25] and Ricaldoni [24] are found, where the stresses and deformations for flat frames are studied when promoting locking by inclined bars/lintels, which refers to us the realistic case of columns braced by horizontal lintels and interlocked by inclined lintels, thus configuring the Z-Bracing System. And, for constructive facilitation, this article also proceeds with the modeling of the X-Bracing System, characterized by lintels with opposite slopes and integrated with each other.

1.1 Research relevance

Bracing of thin-walled columns with an open section is already widespread in the specialized literature, always with the imposition of only horizontal lintels. However, as explained by Ricaldoni [24], and easily verified through structural analysis, it is clear that, when promoting bracing of structural cores through horizontal lintels interlocked by diagonal lintels, the structural launch becomes quite rational and economical. The bracing model exposed by [24], in this article, is called the Z-Bracing System. And for constructive reasons, the X-Bracing System is also analyzed. In particular, for the case of slender columns, there is a lintel bracing system in Z or X, illustrated in Figure 1, whose diagonals greatly reduce the lateral displacements of the aforementioned structural core. In addition, there is evidence of greater locking for the lintels in two mirrored diagonals, right in the X-Bracing System.

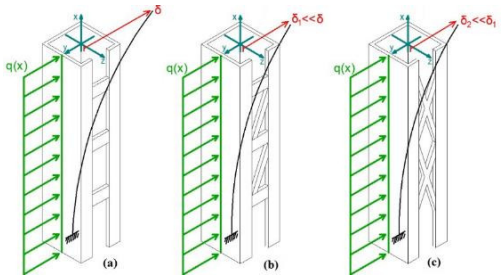

Figure 1: Qualitative exposure of the reduction of lateral displacements in C-cores to (a) conventional bracing, (b) Z-Bracing, and (c) X-Bracing

2 BIBLIOGRAPHICAL REVIEW

It is essential to reinforce that the Continuous Medium Technique (CMT) was widely used from the '70s through the '90s, mainly for static and dynamic analyses of tall buildings. However, with the advent of microcomputers and the technological advancement of software ready for structural analysis via the Finite Element Method (FEM), like ANSYS and TQS, the use of CMT has been relatively overlooked as it requires greater dedication and mathematical equation by structural engineers. Thus, due to the fact alluded to, there is a depression in more recent publications.

2.1 Static analysis of wall panels

CMT publications applied to Tall Buildings did not stop there, they were interspersed with preludes from the 2000s, of which Mancini & Savassi is cited [12]. Then, the CMT was relatively forgotten, being brought back to scientific light by [3], always from the perspective of the Tall Buildings. Subsequently, the complete retrieval of the CMT in Melo [16] was promoted with the static and dynamic modeling of thin-walled columns, braced by horizontal lintels and applied to bridges over deep valleys. As a result of the Thesis immediately cited above, the following scientific articles were published: Melo & Barbosa [17, 18, 19].

In the retrieval of the Flexion-Torsion Theory and consequent application in thin-walled sections, the following are also mentioned: [1, 21]. For the structural cores in C, coupled to the typical structure of tall buildings, [8, 14] are listed. Finally, with emphasis on bracing lintels, the following [7, 10] always stand out for horizontal lintels. As for the X-Bracing System, the modeling is perceived with the plastic hinge simplification in the middle of the gap, mentioning [20, 22].

2.2 Dynamic analysis of the wall panels

To support the dynamic formulations of the thin-walled column modeled via Wall Panel Theory (WPT), it is quite relevant to mention Chitty [2] and Vlassov [30], as well as, Rosman [26], and Laredo [9], where they highlight the possibility of expressing the modes of vibration through the solution of homogeneous spatial HDE (Homogeneous Differential Equation).

3 C-CORE BRACING BY Z LINTELS

Starting from the concepts of bracing in flat frames using inclined lintels crossing the floors of Tall Buildings, as can be seen in Schueller [27], Z-Bracing is seen as a model for redistributing the lateral loads. Adopting the structural analysis procedures recommended in Melo [16], the bracing element in Z lintels is postulated. In Figure 2a, the aforementioned bracing system with the support of the lintels through the Wall Panels (4) and (5) is shown.

Finally, by adapting the formulation postulated for the interaction of the lintels with the Wall Panels, see Szerémi [28], a section of infinite flexion stiffness are adopted in the mentioned segments of interaction, highlighting that the points of convergence of the axes of the lintels are positioned on the axis of the Wall Panels (4) and (5) (see Figure 2b).

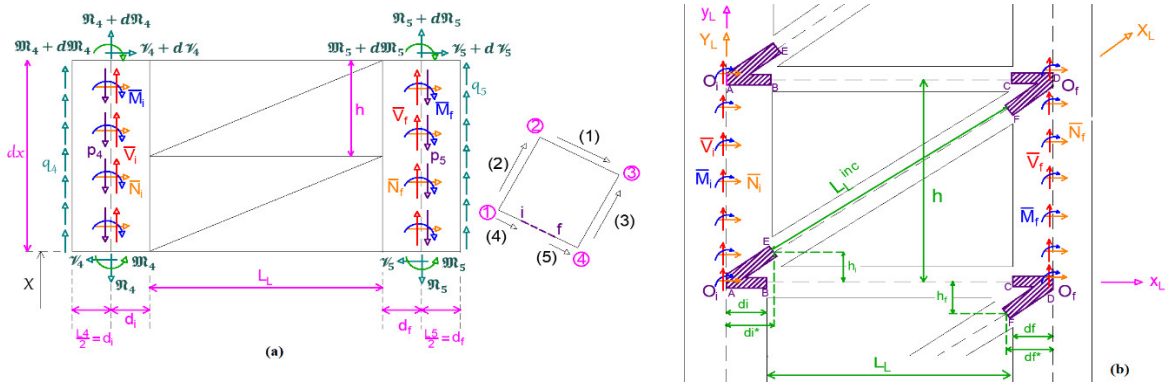

Figure 2: Z-Bracing: (a) System Element and (b) modeling of the structural system of the intersection Z Lintels – Wall Panels

Considering the modeling of lintels through balance equations in internal forces, recommended by Maney [6, 13, 15], among others, Figure 3 postulate the elastic reactions for the horizontal and inclined lintels. This guarantees the structural balance, of which $u_i^L = dH_i^L$, $v_i^L = dR_i^L$, $\theta_i^L = \theta_{G_i}{}^L$, $u_f^L = dH_f^L$, $v_f^L = dR_f^L$, and $\theta s_f^L = \theta_{G_f}{}^L$.

3.1 Correlation equations

Figure 3c shows the deformed state of the lintels, showing the degrees of freedom shown in Figure 3b, in addition to the imposition of elastic reactions, both at the ends of the lintels and the infinitely rigid bars.

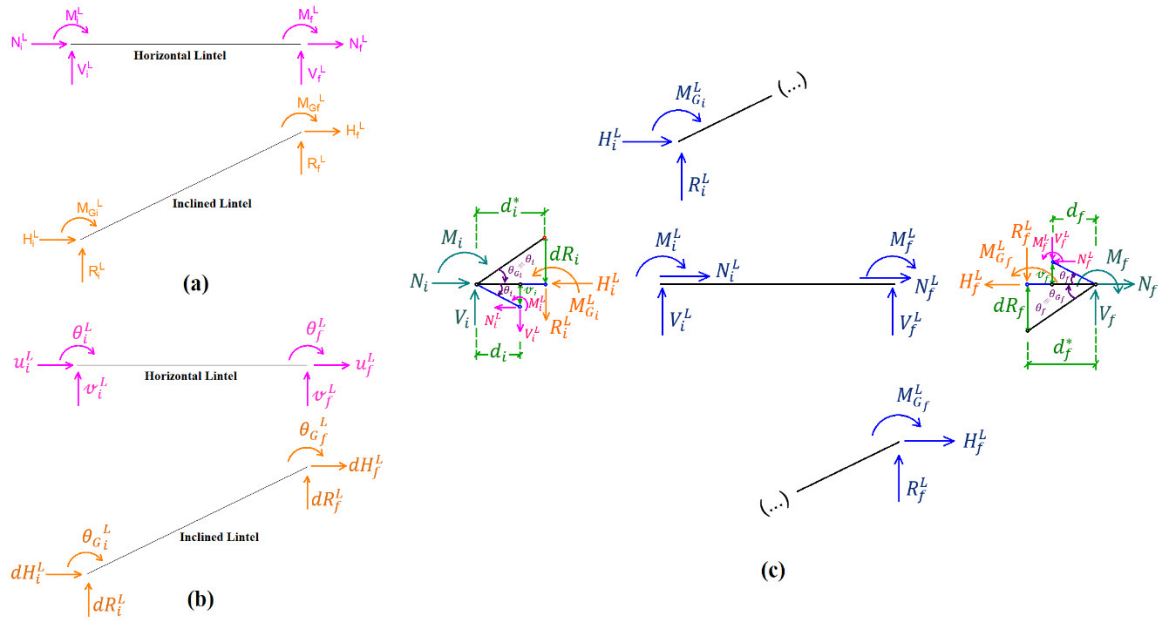

Figure 3: Lintels: (a) elastic reactions, (b) degrees of freedom of the Z-Bracing System and (c) deformed state of the lintels and the resulting elastic reactions

Balancing the convergence points $\boldsymbol{O_i}$ and $\boldsymbol{O_f}$, the matrix organization of the correlation between the elastic reactions at the points of convergence $(\boldsymbol{O_i}$ and $\boldsymbol{O_f})$ with the elastic reactions of the lintels is proceeded, expressed as:

$$\{\boldsymbol{M}\} = \left[\boldsymbol{R_L^{hor}}\right] \cdot \left\{\boldsymbol{M_L^{hor}}\right\} + \left[\boldsymbol{R_L^{inc}}\right] \cdot \left\{\boldsymbol{M_L^{inc}}\right\} \quad (1)$$

with $\left\{M_L^{hor}\right\}^T = \left\{N_i^L \quad V_i^L \quad M_i^L \quad N_f^L \quad V_f^L \quad M_f^L\right\}$, $\left\{M_L^{inc}\right\}^T = \left\{H_i^L \quad R_i^L \quad M_{G_i}^L \quad H_f^L \quad R_f^L \quad M_{G_f}^L\right\}$,

$$\left[R_L^{hor}\right] = \begin{bmatrix} 1 & 0 & 0 & 0 & 0 & 0 \\ 0 & 1 & 0 & 0 & 0 & 0 \\ -v_i & -d_i & 1 & 0 & 0 & 0 \\ 0 & 0 & 0 & 1 & 0 & 0 \\ 0 & 0 & 0 & 0 & 1 & 0 \\ 0 & 0 & 0 & v_f & d_f & 1 \end{bmatrix}, \left[R_L^{inc}\right] = \begin{bmatrix} 1 & 0 & 0 & 0 & 0 & 0 \\ 0 & 1 & 0 & 0 & 0 & 0 \\ v_i^* & -d_i^* & 1 & 0 & 0 & 0 \\ 0 & 0 & 0 & 1 & 0 & 0 \\ 0 & 0 & 0 & 0 & 1 & 0 \\ 0 & 0 & 0 & v_f^* & d_f^* & 1 \end{bmatrix},$$

$\{M\}^T = \{N_i \quad V_i \quad M_i \quad N_f \quad V_f \quad M_f\}$, $v_i^* = (v_i - h_i)$, and $v_f^* = (v_f - h_f)$,

where $\left[R_L^{hor}\right]$ is the correlation matrix between the horizontal lintels and the points of convergence; $\left[R_L^{inc}\right]$ is the correlation matrix between the inclined lintels and the points of convergence; $\{M\}$ is the elastic reaction vector at the points of convergence; $\left\{M_L^{hor}\right\}$ is the elastic reaction vector on the horizontal lintels; and $\left\{M_L^{inc}\right\}$ is the elastic reaction vector on the inclined lintels.

3.2 Balance equations of the lintels

From the Maney equations to the Finite Element of horizontal and inclined bars, together with the notation employed in Figure 3a and Figure 3c, the following is written:

$$\left\{\boldsymbol{M_L^{hor}}\right\} = \left[\boldsymbol{k_L^{hor}}\right] \cdot \left\{\boldsymbol{d_L^{hor}}\right\} \quad (2)$$

$$\left\{\boldsymbol{M_L^{inc}}\right\} = \left[\boldsymbol{k_L^{inc}}\right] \cdot \left\{\boldsymbol{d_L^{inc}}\right\} \quad (3)$$

with: $k_i^L = k_f^L = k^L, a^L, r^L, t^L, b_i^L = b_f^L = b^L, k_i^{inc} = k_f^{inc} = k^{inc}, a^{inc}, r^{inc}, t^{inc}, b_i^{inc}, b_f^{inc}$, $b_i^{*inc}, b_f^{*inc}, r^{*inc}$ are Mane's coefficients, see [1, 13], where $\left\{d_L^{hor}\right\}^T \equiv \left\{d_L^{inc}\right\}^T = \{u_i \quad v_i \quad \theta_i \quad u_f \quad v_f \quad \theta_f\}$, k_c being the form factor.

3.3 Elastic reaction transfer

The transformation of the referential is carried out, starting from the ends of the lintels to the points of convergence $\boldsymbol{O_i}$ and $\boldsymbol{O_f}$, located on the axis of the Wall Panels (4) and (5), respectively. Which will imply three successive transformations of reference, namely:

3.3.1 First transformation

From the displacement vector $\{\boldsymbol{d^L}\}$ at the ends of the lintels, towards the displacement vector at the points of convergence, results in $\{d\}^T = \{u_i \quad v_i \quad \theta_i \quad u_f \quad v_f \quad \theta_f\}$ and $\{d^L\}^T = \left\{u_i^L \quad v_i^L \quad \theta_i^L \quad u_f^L \quad v_f^L \quad \theta_f^L\right\} \equiv \{d\}^T$. To keep the structural balance, the following is written: $\{d\} = [I] \cdot \{d^L\}$.

3.3.2 Second transformation

A correlation is established between the degrees of freedom of the lintel ends with those of the convergence points, as shown in the following three steps:

- *1st Stage:* The Global Coordinate System (GCS) is initially defined for degrees of freedom at points of convergence, expressing vector $\{\boldsymbol{D}\}$ by:

$$\{D\}^T = \{\bar{u}_i \quad \bar{v}_i \quad \bar{\theta}_i \quad \bar{u}_f \quad \bar{v}_f \quad \bar{\theta}_f\} \tag{4}$$

as illustrated in Figure 4.

- *2nd Stage:* Correlating the Degrees of Freedom vector of the horizontal lintel $\{\boldsymbol{d_L^{hor}}\}$ with the Degrees of Freedom vector at the points of convergence $\{\boldsymbol{D}\}$. And for that end, it considers Figure 4a.

Proceeding, now, the balance of sections AB and CD, of stiffness considered as infinite, there is $\bar{u}_i = u_i^L \equiv u_i$, $\bar{v}_i = v_i^L \equiv v_i$, $\bar{\theta}_i = \theta_i^L - (v_i) \cdot u_i^L - (d_i).v_i^L \equiv \theta_i - v_i \cdot u_i - d_i \cdot v_i$, $\bar{u}_f = u_f^L \equiv u_f$, $\bar{v}_f = v_f^L \equiv v_f$ and $\bar{\theta}_f = \theta_f + v_f \cdot u_f + d_f \cdot v_f$. Which, in a matrix form, is expressed by $\{D\} = \left[R_L^{hor}\right] \cdot \left\{d_L^{hor}\right\}$. And finally, inverting equation results in:

$$\left\{\boldsymbol{d_L^{hor}}\right\} = \left[\boldsymbol{R_L^{hor}}\right]^{\boldsymbol{T}} \cdot \{\boldsymbol{D}\} \tag{5}$$

- *3rd Stage:* Correlating the Degrees of Freedom vector of the inclined lintel $\{d_L^{inc}\}$ with the Degrees of Freedom vector at the points of convergence $\{D\}$. And for that end, it considers Figure 4b.

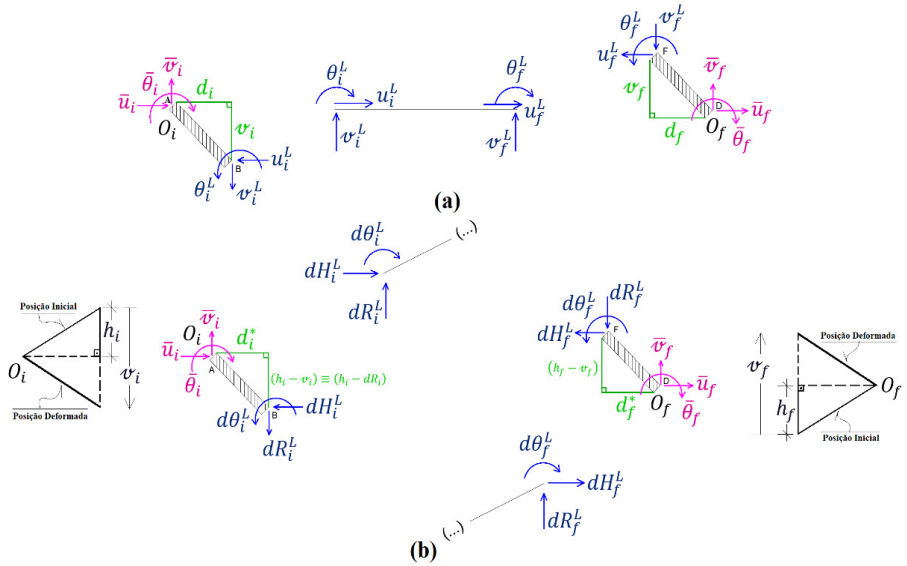

Figure 4: Displacements v_i and v_f in: (a) the horizontal lintel and (b) the inclined lintel

Proceeding, now, the balance of sections AB and CD, of stiffness considered as infinite matrix form, is expressed by: $\{D\} = \left[R_L^{inc}\right] \cdot \left\{d_L^{inc}\right\}$. And finally, inverting Eq. (5) results in:

$$\left\{\boldsymbol{d_L^{inc}}\right\} = \left[\boldsymbol{R_L^{inc}}\right]^{\boldsymbol{T}} \cdot \{\boldsymbol{D}\} \tag{6}$$

3.3.3 Third transformation

Passing the stiffness of the lintels to the Global Coordinate System (GCS), thus computing the stiffness of the Z-Bracing System. Initially, applying Eq. (2) and (3) in Eq. (1), we obtain:

$$\{\boldsymbol{M}\} = \left[\boldsymbol{R_L^{hor}}\right] \cdot \left[\boldsymbol{k_L^{hor}}\right] \cdot \left\{\boldsymbol{d_L^{hor}}\right\} + \left[\boldsymbol{R_L^{inc}}\right] \cdot \left[\boldsymbol{k_L^{inc}}\right] \cdot \left\{\boldsymbol{d_L^{inc}}\right\} \tag{7}$$

Then, imposing Eq. (5) and (6) in Eq. (7), the rigidities are written in the Global Coordinate System, but without computing the incidence of the lintels. Thus, Eq. (7) is rewritten as:

$$\{\boldsymbol{M}\} = \left[\boldsymbol{R_L^{hor}}\right] \cdot \left[\boldsymbol{k_L^{hor}}\right] \cdot \left[\boldsymbol{R_L^{hor}}\right]^{\boldsymbol{T}} \cdot \{\boldsymbol{D}\} + \left[\boldsymbol{R_L^{inc}}\right] \cdot \left[\boldsymbol{k_L^{inc}}\right] \cdot \left[\boldsymbol{R_L^{inc}}\right]^{\boldsymbol{T}} \cdot \{\boldsymbol{D}\} \tag{8}$$

3.3.4 Fourth transformation

The incidences of the lintels are computed and the stiffness matrix of the Z-Bracing System is assembled, making the following five steps operational:

- *1st Stage:* Defining the finite element of the Z-Bracing System, through Figure 5, considering the auxiliary points 3 and 4 diagonally located in the center of the lintels.

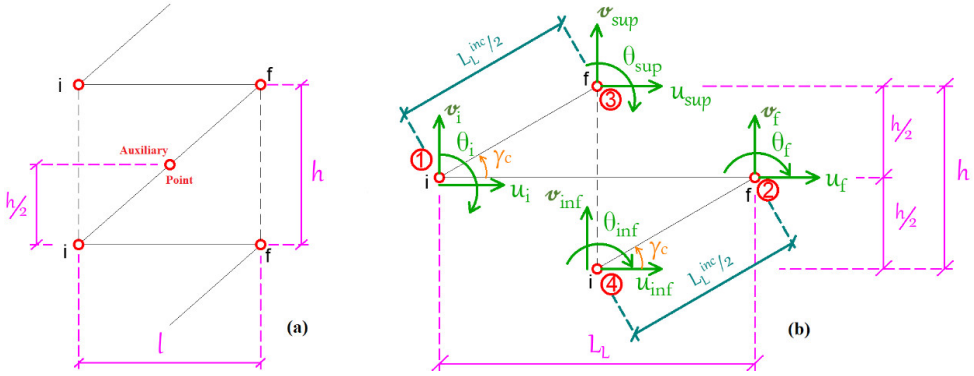

Figure 5: Finite element of the Z-Bracing system: (a) positioning of the auxiliary points and (b) FE with the indication of the degrees of freedom, quotas and numbering of nodes for Matrix Analysis

- *2nd Stage:* Beginning of the Matrix Analysis of Structures (MAS) of the system shown in Figure 5b, starting from the stiffness matrices in the GCS and considering the incidence of lintels in the bracing system shown in Figure 5. Highlighting that, on this stage, the Stiffness Matrix $\left[\boldsymbol{k_L^{inc}}\right]$ imposes half the length L_L^{inc} in the auxiliary formulas shown in Eq. (3). And it is noteworthy that [β] are the Incidence Matrices of the lintels shown in Figure 5b.
- *3rd Stage:* Processing the products pointed out in $\left[k_L^{hor}\right]^*$; $\left[k_L^{sup}\right]^*$; $\left[k_L^{inf}\right]^*$, in addition to adopting the MAS.
- *4th Stage:* Applying the Matrix Condensation in systems:

$\left\{M_L^{sup}\right\} = \left[k_L^{sup}\right]^* \cdot \left\{d_L^{sup}\right\}$ e $\left\{M_L^{inf}\right\} = \left[k_L^{inf}\right]^* \cdot \left\{d_L^{inf}\right\}$, expresses one of the two plots that compose the Global Balance of the Bracing, thus expressed in two substages:

- Assembling the matrix equations of the non-condensed systems:

$$\{M\}_1 = [k_L^{inc}]_{I,I} \cdot \{d\}_1 + [k_L^{inc}]_{I,II} \cdot \{d\}_3, \qquad \{M\}_3 = [k_L^{inc}]_{II,I} \cdot \{d\}_1 + [k_L^{inc}]_{II,II} \cdot \{d\}_3$$

$$\{M\}_2 = [k_L^{inc}]_{II,II} \cdot \{d\}_2 + [k_L^{inc}]_{II,I} \cdot \{d\}_4, \quad \{M\}_4 = [k_L^{inc}]_{I,II} \cdot \{d\}_2 + [k_L^{inc}]_{I,I} \cdot \{d\}_4;$$

- Finally, grouping $\{M\}_1, \{M\}_2, \{M\}_3$ and $\{M\}_4$, considering that there is no application of external loads at points 3 and 4 that are shown in Figure 5b, is expressed as:

$$\begin{Bmatrix} \{M\}_1 \\ \{M\}_2 \end{Bmatrix} = \begin{bmatrix} [k_L^{inc}]_{I,I}^* & [0] \\ [0] & [k_L^{inc}]_{II,II}^* \end{bmatrix} \cdot \begin{Bmatrix} \{d\}_1 \\ \{d\}_2 \end{Bmatrix} \tag{9}$$

➢ *5th Stage:* Composing the Stiffness Matrix of the Z-Bracing System, grouping Eq. (9) and the system expressed in Eq. (8), via the correlation matrices, thus, forming the Global Balance System of the Bracing System, which is expressed by:

$$\{\boldsymbol{M}\} = [\boldsymbol{K}].\{\boldsymbol{D}\} \tag{10}$$

with $[K] = \begin{bmatrix} [K]_{I,I} & [K]_{I,II} \\ [K]_{II,I} & [K]_{II,II} \end{bmatrix}$ *and* $[k_L^{hor}]^{**} = \begin{bmatrix} [k_L^{hor}]_{I,I} & [k_L^{hor}]_{I,II} \\ [k_L^{hor}]_{II,I} & [k_L^{hor}]_{II,II} \end{bmatrix}$,

or even $[K] = [R_L^{hor}] \cdot [k_L^{hor}]^{**} \cdot [R_L^{hor}]^T + [R_L^{inc}] \cdot [k_L^{inc}]^* \cdot [R_L^{inc}]^T$,

where $[K]_{I,I} = [R_L^{hor}]_{I,I} \cdot [k_L^{hor}]_{I,I} \cdot [R_L^{hor}]_{I,I} + [R_L^{inc}]_{I,I} \cdot [k_L^{inc}]_{I,I}^* \cdot [R_L^{inc}]_{I,I}$,

$[K]_{I,II} = [R_L^{hor}]_{I,I} \cdot [k_L^{hor}]_{I,II} \cdot [R_L^{hor}]_{II,II}$; $\quad [K]_{II,I} = [R_L^{hor}]_{II,II} \cdot [k_L^{hor}]_{II,I} \cdot [R_L^{hor}]_{I,I}$, and

$[K]_{II,II} = [R_L^{hor}]_{II,II} \cdot [k_L^{hor}]_{II,II} \cdot [R_L^{hor}]_{II,II} + [R_L^{inc}]_{II,II} \cdot [k_L^{inc}]_{II,II}^* \cdot [R_L^{inc}]_{II,II}$.

3.4 Elastic reaction on wall panels

Figure 6a and Figure 6b shows the transformation of the elastic reactions concentrated in the points of convergence $(\boldsymbol{O_i}$ e $\boldsymbol{O_f})$ in elastic reactions distributed in the Continuous Medium. Finally, using Eq. (10), the Continuous Medium elastic reactions result in:

$$\begin{Bmatrix} N_i \\ V_i \\ M_i \\ N_f \\ V_f \\ M_f \end{Bmatrix} = \begin{bmatrix} K_{11} & K_{12} & K_{13} & K_{14} & K_{15} & K_{16} \\ K_{21} & K_{22} & K_{23} & K_{24} & K_{25} & K_{26} \\ K_{31} & K_{32} & K_{33} & K_{34} & K_{35} & K_{36} \\ K_{41} & K_{42} & K_{43} & K_{44} & K_{45} & K_{46} \\ K_{51} & K_{52} & K_{53} & K_{54} & K_{55} & K_{56} \\ K_{61} & K_{62} & K_{63} & K_{64} & K_{65} & K_{66} \end{bmatrix} \cdot \begin{Bmatrix} u_i \\ v_i \\ \theta_i \\ u_f \\ v_f \\ \theta_f \end{Bmatrix} \tag{11}$$

The elastic reactions in the Continuous Medium are written as: $\overline{\boldsymbol{N}}_{\boldsymbol{i}} = \frac{\boldsymbol{N_i}}{\boldsymbol{h}}$, $\overline{\boldsymbol{V}}_{\boldsymbol{i}} = \frac{\boldsymbol{V_i}}{\boldsymbol{h}}$, $\overline{\boldsymbol{M}}_{\boldsymbol{i}} = \frac{\boldsymbol{M_i}}{\boldsymbol{h}}$, $\overline{\boldsymbol{N}}_{\boldsymbol{f}} = \frac{\boldsymbol{N_f}}{\boldsymbol{h}}$, $\overline{\boldsymbol{V}}_{\boldsymbol{f}} = \frac{\boldsymbol{V_f}}{\boldsymbol{h}}$ and $\overline{\boldsymbol{M}}_{\boldsymbol{f}} = \frac{\boldsymbol{M_f}}{\boldsymbol{h}}$. Through Figure 6c and Figure 6d, the deformations u_i; u_f; v_i; v_f; θ_i e θ_f are expressed in terms of the Flexion-Torsion Theory (FTT), explicitly stating the

calculations of the sectorial ordinates ω_i and ω_f. The degrees of freedom are expressed by: $u_i = -v_i$; $v_i = \omega_i.\phi'$; $\theta_i = \frac{\omega_i}{d_i}.\phi'$; $u_f = -v_f$; $v_f = \omega_f.\phi'$; $\theta_f = \frac{\omega_f}{d_f}.\phi'$.

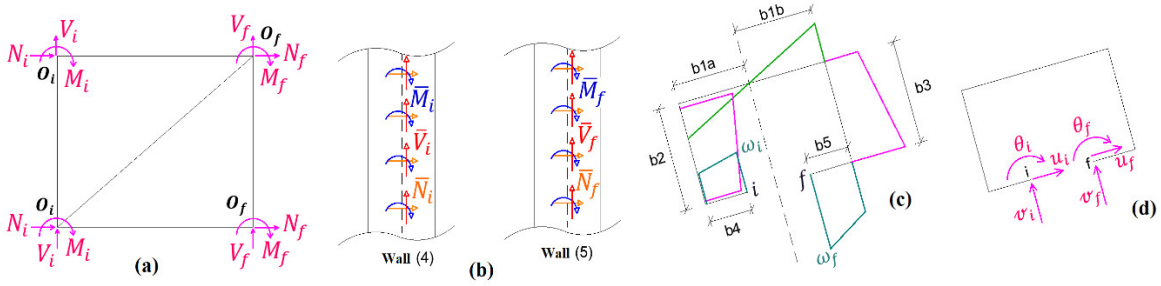

Figure 6: Z-Bracing system: (a) elastic reactions, (b) elastic reactions distributed in the Continuous Medium, (c) sectorial coordinate and (d) degrees of freedom.

4 C-CORE X-BRACING BY LINTELS

Figure 7a shows the configuration of the double diagonal lintels opposite each other, called X-Bracing System, considering the infinitely rigid sections, the dimensions, the local axes of the Local Coordinate System (LCS), besides the elastic reactions distributed in the Continuous Medium. Figure 7b and Figure 7c show the degrees of freedom and the elastic reactions for the referred bracing system, whose lintel lengths are expressed by $\ell_a = \frac{\ell}{2.\cos(\gamma_a)} - \frac{h_d}{2} - \frac{h_a}{tg(\gamma_a)}$ and $\ell_d = \frac{\ell}{2.\cos(\gamma_d)} - \frac{h_a}{2} + \frac{h_d}{tg(\gamma_d)}$.

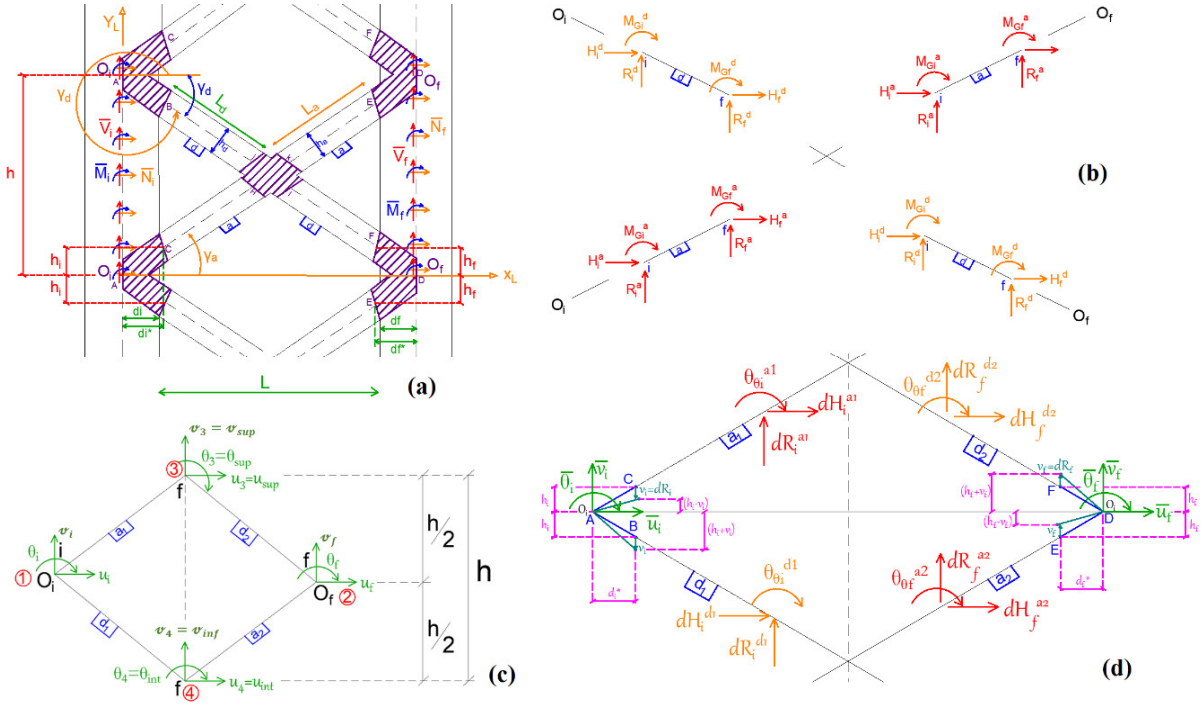

Figure 7: X-Bracing system: (a) with the notation of the lintels, (b) elastic reactions, (c) degrees of freedom and (d) elastic reactions and the deformed state of the X lintels.

4.1 Correlation equations

Based on Figure 7d, where the deformed state of the lintels in X is shown, the elastic reactions are highlighted, which, in a matrix form, expresses the balance of the elastic reactions, shown in Figure 7d, as:

$$\{M\} = [R_L^a] \cdot \{M_L^a\} + [R_L^d] \cdot \{M_L^d\} \tag{12}$$

4.2 Lintel balance equations

The application of Maney´s equations in the ascending and descending lintels shown in Figure 7b and Figure 7d results in:

$$\begin{gathered} \{M_L^{a_1}\} = [k_L^a].\{d_L^{a_1}\}, \{M_L^{d_1}\} = [k_L^d].\{d_L^{d_1}\}, \\ \{M_L^{a_2}\} = [k_L^a].\{d_L^{a_2}\} \text{ and } \{M_L^{d_2}\} = [k_L^d].\{d_L^{d_2}\} \end{gathered} \tag{13}$$

4.3 Elastic reaction transfer

The elastic reactions are transferred from the ends of the lintels to the points of convergence $(O_i$ and $O_f)$, considering the finite element shown in Figure 7b.

4.3.1 First transformation

It is carried out from the displacement vector $\{d_L\}$ to $\{d\}$, where $\{d_L^{a_1}\}$, $\{d_L^{a_2}\}$, $\{d_L^{d_1}\}$ and $\{d_L^{d_2}\}$ are the vectors of the degrees of freedom in lintels a_1, a_2, d_1 and d_2, respectively.

4.3.2 Second transformation

The degrees of freedom are correlated at the ends of the lintels with the points of convergence. This is done through sections of infinite stiffness, see Figure 7d. The following two steps are considered for this procedure:

- *1st Stage:* Defining the Global Coordinate System for degrees of freedom at points of convergence, which, by the way, coincide with those highlighted in Figure 7d.
- *2nd Stage:* Correlating vectors $\{d_L\}$, by lintel, with the vector $\{D\}$, using displacements v_i and v_f in the stiffness sections considered to be infinite.

4.3.3 Third transformation

The stiffness of the LCS is transformed into the Global Coordinate System (GCS), in addition to processing the union of the X-Bracing System, as shown in the following four steps.

- *1st Stage:* Defining the auxiliary points and delimiting the finite element of the X-Bracing system, using Figure 7c.
- *2nd Stage:* Applying Matrix Condensation to the matrices, keeping the eye on the finite bracing element that is shown in Figure 7c, for systems: $\{M_L^{a_1}\} =$

$\left[k_L^{a_1}\right]^* \cdot \{d_L^{a_1}\}$, $\{M_L^{a_2}\} = \left[k_L^{a_2}\right]^* \cdot \{d_L^{a_2}\}$, $\{M_L^{d_1}\} = \left[k_L^{d_1}\right]^* \cdot \{d_L^{d_1}\}$ and $\{M_L^{d_2}\} = \left[k_L^{d_2}\right]^* \cdot \{d_L^{d_2}\}$.

- *3rd Stage:* By imposing the correlation matrices $[R_L^a]$ and $\left[R_L^d\right]$, the stiffness matrices referenced in the convergence centers are written as follows: $[k_L^a]^{**} = [R_L^a] \cdot [k_L^a]^* \cdot [R_L^a]^T$ and $\left[k_L^d\right]^{**} = \left[R_L^d\right] \cdot \left[k_L^d\right]^* \cdot \left[R_L^d\right]^T$.
- *4th Stage:* Finally, unify the stiffness by adding $[k_L^a]^{**}$ and $\left[k_L^d\right]^{**}$, expressed as:

$$\{\boldsymbol{M}\} = [\boldsymbol{K}].\{\boldsymbol{D}\} \quad \therefore \quad \{\boldsymbol{M}\} = \left([\boldsymbol{k_L^a}]^{**} + \left[\boldsymbol{k_L^d}\right]^{**}\right).\{\boldsymbol{D}\} \tag{14}$$

4.4 Elastic reactions in the wall panel centers (4) and (5)

Initially, the correlation matrices $\left[R_{L_i}\right]$ and $\left[R_{L_f}\right]$ are rewritten for the ascending and descending lintels. In this way, plots v_i and v_f, are canceled, since in Eq. (14) there are products that lead to ${v_i}^2$, $v_i.u_i$, ..., $v_i.\theta_i$, which, via FTT, are adopted as null. Thus, the correlation matrices are expressed as:

$$\left[R_{L_i}^a\right] = \begin{bmatrix} 1 & 0 & 0 \\ 0 & 1 & 0 \\ h_i & -d_i^* & 1 \end{bmatrix}, \left[R_{L_f}^a\right] = \begin{bmatrix} 1 & 0 & 0 \\ 0 & 1 & 0 \\ -h_f & d_f^* & 1 \end{bmatrix}, \left[R_{L_i}^d\right] = \begin{bmatrix} 1 & 0 & 0 \\ 0 & 1 & 0 \\ -h_i & -d_i^* & 1 \end{bmatrix} \text{ and } \left[R_{L_f}^d\right] = \begin{bmatrix} 1 & 0 & 0 \\ 0 & 1 & 0 \\ h_f & d_f^* & 1 \end{bmatrix}.$$

Figure 8 shows the conversion of the finite element for the continuous system of elastic reactions. The elastic reactions in the Continuous Medium are written via Eq. (11) with: $K_{1,i} = K_{2,i} = K_{3,i} = 0, K_{4,j} = K_{5,j} = K_{6,j} = 0 \; and \; i = \{4,5,6\}, j = \{1,2,3\}$.

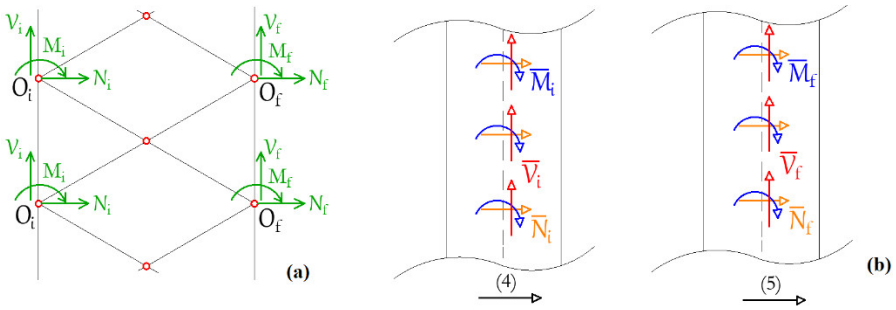

Figure 8: X-Bracing system: (a) FE with the nodal elastic reactions under the points of convergence O_i and O_f and (b) elastic reactions distributed in the continuous medium

5 WALL PANEL EQUATING

Figure 9a shows the numbering of the Wall Panels, from (1) to (5), as well as the direction adopted for modeling. It also presents the directions of shear flow at the intersections, in addition to exposing in detail the differential elements of the aforementioned wall panels, through CMT. The lateral loads $({q_1}^*, {q_2}^*$ and $Q)$ are highlighted in Figure 9b.

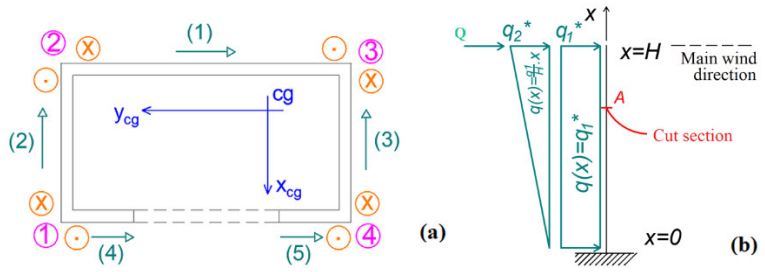

Figure 9: Thin-walled column: (a) adopted convention and (b) Lateral loading to simulate wind action

To this end, internal forces are balanced, displacements are made compatible at intersections, and the balance of shear forces. From this procedure, the following is obtained as a system of differential equations, which represents the static forces of the C-columns braced in Z and X, and referenced in the Center of Gravity:

$$-[J]_{3x3} \cdot \{v'''_{CG}(x)\} + [S]_{3x3} \cdot \{v'_{CG}(x)\} = \{V_{f_{CG}}(x)\}_{3x1} \tag{15}$$

where $[S] = [M_9]^T.([M_6] + [M_8].[M_1]^{-1}.[M_2]) + [M_{11}]$, $[M_2] = \begin{bmatrix} 0 & 0 & d_1^* \\ 0 & 0 & 0 \\ 0 & 0 & 0 \\ 0 & 0 & d_2^* \end{bmatrix}$, $[M_6] = \begin{bmatrix} 0 & 0 & 0 \\ 0 & 0 & 0 \\ 0 & 0 & d_3^* \\ 0 & 0 & d_4^* \end{bmatrix}$,

$$d_1^* = -\frac{A_2}{h} \cdot \left\{ \omega_i \cdot \left(-K_{21} + K_{22} + \frac{K_{23}}{d_i} \right) + \omega_f \cdot \left(-K_{24} + K_{25} + \frac{K_{26}}{d_f} \right) \right\}, \quad \text{with: } K_{24} = K_{25} = K_{26} = 0 \text{ for the X-Bracing System,}$$

$$d_2^* = -\frac{A_3}{h} \cdot \left\{ \omega_i \cdot \left(-K_{51} + K_{52} + \frac{K_{53}}{d_i} \right) + \omega_f \cdot \left(-K_{54} + K_{55} + \frac{K_{56}}{d_f} \right) \right\}, \quad \text{with: } K_{51} = K_{52} = K_{53} = 0 \text{ for the X-Bracing System,}$$

$$d_3^* = -\frac{1}{h} \cdot \left\{ \omega_i \cdot \left(-K_{31} + K_{32} + \frac{K_{33}}{d_i} \right) + \omega_f \cdot \left(-K_{34} + K_{35} + \frac{K_{36}}{d_f} \right) \right\}, \quad \text{with: } K_{34} = K_{35} = K_{36} = 0 \text{ for the X-Bracing System,}$$

$$d_4^* = -\frac{1}{h} \cdot \left\{ \omega_i \cdot \left(-K_{61} + K_{62} + \frac{K_{63}}{d_i} \right) + \omega_f \cdot \left(-K_{64} + K_{65} + \frac{K_{66}}{d_f} \right) \right\}, \quad \text{with: } K_{61} = K_{62} = K_{63} = 0 \text{ for the X-Bracing System.}$$

The first evidence that should be made in the dynamic analysis of reinforced concrete structural cores is the fact that the differential equation of the static plot is referenced in the Center of Gravity (CG), while the dynamic plot refers, at first, to the Center of Mass (CM). From the explicit correlations resulting from the transfer process of the degrees of freedom from CG to D, for the thin-walled column, according to Melo [16], the WPT dynamic analysis system of differential equations referenced in D is written as:

$$-[\bar{J}] \cdot \{v''''_D(x,t)\} + [\bar{S}] \cdot \{v''_D(x,t)\} + [\bar{\bar{M}}] \cdot \{\ddot{v}_D(x,t)\} = \{\bar{V}'_f(x,t)\} \tag{16}$$

with $\{v_{CG}\} = [T] \cdot \{v_D\}$, $[T] = \begin{bmatrix} 1 & 0 & -z_{CG} \\ 0 & 1 & y_{CG} \\ 0 & 0 & 1 \end{bmatrix}$ and $[\bar{T}_M] = \begin{bmatrix} 1 & 0 & -d_{z_{CM-CG}} \\ 0 & 1 & d_{y_{CM-CG}} \\ 0 & 0 & 1 \end{bmatrix}$.

5.1 Dynamic system decoupling

Following the concepts recommended in [23] regarding the Diagonalization Method postulated by Jacobi; and [17], Figure 10 shows the system decoupling flowchart present in Eq. (16), where the terms are described by:

$$[R_e] = \begin{bmatrix} \cos(\phi_R) & -\operatorname{sen}(\phi_R) & z_R \\ \operatorname{sen}(\phi_R) & \cos(\phi_R) & y_R \\ 0 & 0 & 1 \end{bmatrix} \tag{17}$$

where $\phi_R = \frac{1}{2} \cdot tg^{-1}\left(\frac{2.\bar{J}_{12}}{\bar{J}_{11}-\bar{J}_{22}}\right)$, $y_R = \frac{-\bar{J}_{13}.\bar{J}_{12}+\bar{J}_{23}.\bar{J}_{11}}{\bar{J}_{11}.\bar{J}_{22}-(\bar{J}_{12})^2}$ and $z_R = \frac{-\bar{J}_{13}.\bar{J}_{22}+\bar{J}_{23}.\bar{J}_{12}}{\bar{J}_{11}.\bar{J}_{22}-(\bar{J}_{12})^2}$.

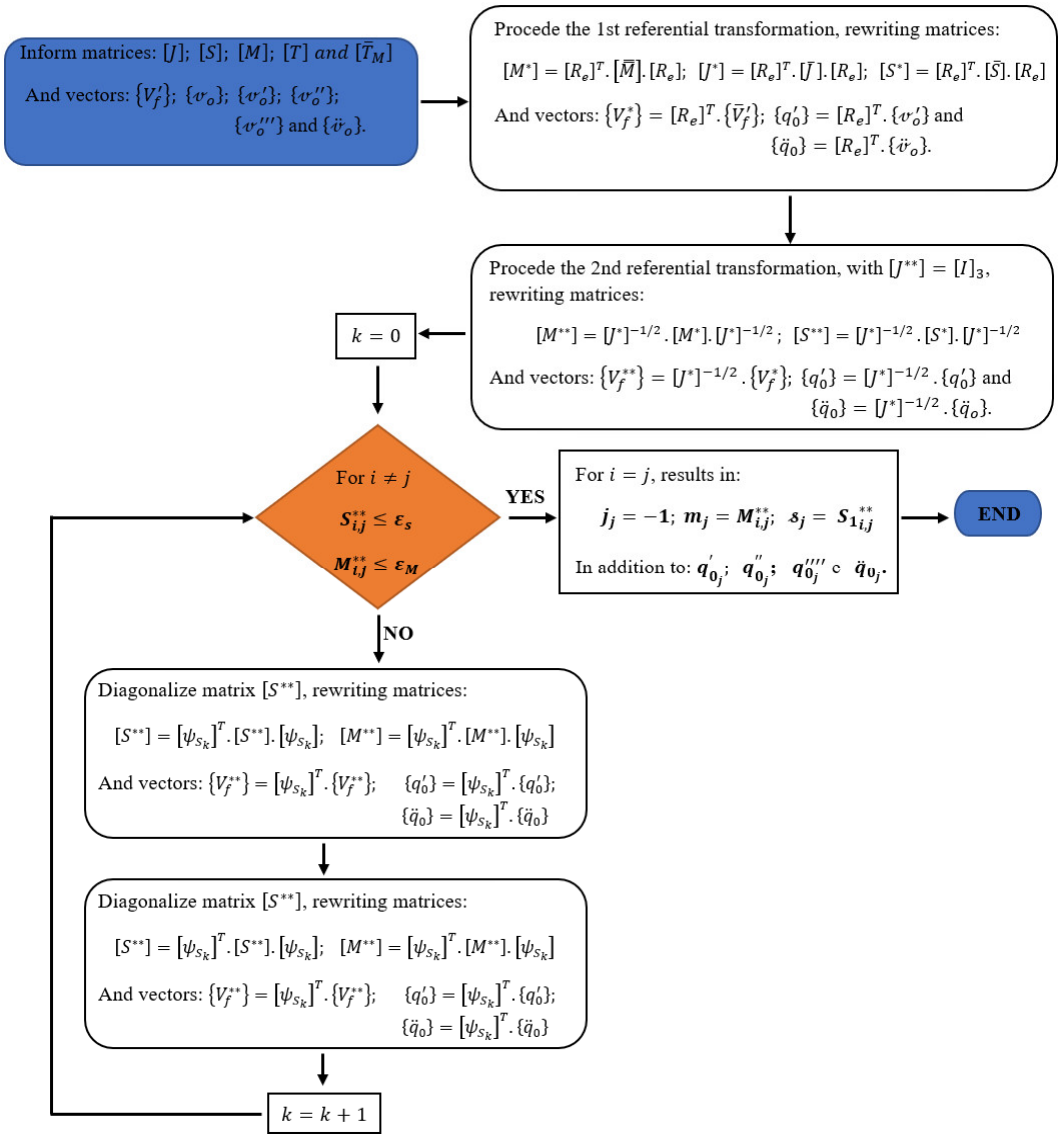

Figure 10: Flowchart of the decoupling of the system in the dynamic force at the WPT, whose complementary information are in Eq. (17)

After the diagonalization process of the matrices of the WPT differential equation system, under dynamic forces, the set is written with three decoupled equations, for j = {1; 2 and 3}, as:

$$-q_j''''(\bar{x},t) + s_j \cdot q_j''(\bar{x},t) + m_j \cdot \ddot{q}_j(\bar{x},t) = \bar{V}_{f_j}(\bar{x},t) \tag{18}$$

6 MODAL ANALYSIS OF THE WALL PANELS

Following the principles advocated in Volterra & Zachmanoglou [31], the modal analysis of Eq. (18) proceeds through its homogeneous. Next, the Variable Separation Process is applied, resulting in two ordinary differential equations, one spatial and one temporal, expressed by: $-\boldsymbol{u}''''(\overline{\boldsymbol{x}}) + \boldsymbol{s} \cdot \boldsymbol{u}''(\overline{\boldsymbol{x}}) - \boldsymbol{\omega}^2 \cdot \boldsymbol{u}(\overline{\boldsymbol{x}}) = \boldsymbol{0}$; $\boldsymbol{m} \cdot \ddot{\boldsymbol{g}}(\boldsymbol{t}) - \boldsymbol{\omega}^2 \cdot \boldsymbol{g} = \boldsymbol{0}$.

Finally, expressing the first seven modes of vibration, in light of ratio λ $\left(\lambda^2 = {\lambda_4}^2 - {\lambda_1}^2\right)$, as shown in Table 1, where H is the height of the column, and s is equivalent to values s_{11}, s_{22} or s_{33} originating from the diagonalization process of the stiffness matrix $[S]$ of the bracing system. Calculating $\lambda = H.\sqrt{s}$ to proceed with the use of the CMT table and the generation of the table, ${\omega_j}^* = {\lambda_1}_j.{\lambda_4}_j$ e ${T_j}^* = \frac{2\pi}{{\omega_j}^*}$ is also used.

Table 1: Frequency and period of the first modes of vibration for the Z and X braced thin-walled column in light of relation λ [16].

λ		$i=1$	$i=2$	$i=3$	$i=4$	$i=5$	$i=6$
2.5	λ_1	2.17092	4.90452	8.03356	9.23096	10.12354	11.68447
	λ_4	1.48758	4.64266	7.87643	9.09454	9.99930	11.57700
	ω_i^*	3.22942	22.77003	63.27574	83.95132	101.22834	135.27106
	f_i^*	0.51398	3.62398	10.07049	13.36184	16.11084	21.52852
7.5	λ_1	2.89825	5.30895	8.29810	9.50762	10.32883	11.82274
	λ_4	0.94861	4.54807	7.83316	9.10466	9.95915	11.50118
	ω_i^*	2.74930	24.14548	65.00038	86.56365	102.86640	135.97548
	f_i^*	0.43756	3.84290	10.34554	13.77790	16.37197	21.64033
15.0	λ_1	3.91350	5.88096	8.68511	9.90673	10.63608	11.96891
	λ_4	0.56168	4.42557	7.77375	9.11829	9.90587	11.32496
	ω_i^*	2.19813	26.02661	67.51584	90.33248	105.35959	135.54747
	f_i^*	0.34984	4.14233	10.74576	14.37610	16.76727	21.57497

7 RESULTS AND DISCUSSIONS

7.1 Aplication 1

In this first numerical example, a column with height H = 100 m, with a cross-section in the shape of a structural C-core, molded with reinforced concrete, is modeled, whose dimensions are $b_1 = b_2 = b_3 = 3.45$ m and $b_4 = b_5 = 1.00$ m for the Wall Panels shown in Figure 9a. It is also admitted that the thickness is t = 0.25 m and reinforced concrete with characteristic resistance to compression is used as material: $f_{ck} = 50$ MPa, imposing the following loads as loading, as shown in Figure 9b, $q_1 = 50\frac{\text{kN}}{\text{m}}$, $q_2 = 0\frac{\text{kN}}{\text{m}}$, and $Q = 0$ kN. The Z-Bracing dimensions are also explained, according to the notation presented in Figure 2b, and expressed by $L_L = 1.45$ m, $L_L^{inc} = 4.73$ m, $h = 5$ m, $d_i = d_f = 0.50$ m, $d_i^* = d_f^* = 0.3729$ m and $h_i = h_f = 0.55$ m, with slope $\gamma_c = 72.14^{\circ}$ for diagonal lintels. The following remains in the system of differential equations of dynamic analysis in the CG:

$$\begin{bmatrix} J_a & 0 & J_d \\ 0 & J_b & J_e \\ J_d & J_e & J_c \end{bmatrix} \cdot \begin{Bmatrix} v_{CG}'''' \\ \omega_{CG}'''' \\ \phi_{CG}'''' \end{Bmatrix} + \begin{bmatrix} 0 & 0 & S_a \\ 0 & 0 & S_b \\ 0 & 0 & S_c \end{bmatrix} \cdot \begin{Bmatrix} v_{CG}'' \\ \omega_{CG}'' \\ \phi_{CG}'' \end{Bmatrix} + \begin{bmatrix} M_a & 0 & M_d \\ 0 & M_b & M_e \\ M_d & M_e & M_c \end{bmatrix} \cdot \begin{Bmatrix} \ddot{v}_{CG} \\ \ddot{\omega}_{CG} \\ \ddot{\phi}_{CG} \end{Bmatrix} = \begin{Bmatrix} V_a' \\ V_b' \\ V_c' \end{Bmatrix} \qquad (19)$$

with $J_a = 2.685 \cdot 10^8$, $J_b = 2.233 \cdot 10^8$, $J_c = 4.05 \cdot 10^8$, $J_d = -5.004 \cdot 10^7$, $J_e = 5.96 \cdot$

10^{-8}, $S_a = 1.712 \cdot 10^5$, $S_b = -7.349 \cdot 10^4$, $S_c = 7.312 \cdot 10^5$, $M_a = 7.871 \cdot 10^3$, $M_b = 7.871 \cdot 10^3$, $M_c = 314.754$, $M_d = 387.785$, $M_e = 1.506 \cdot 10^3$, $V_a' = -50$, $V_b' = 0$ and $V_c' = -185.024$. And after applying the decoupling flowchart, shown in Figure 10, the set of decoupled differential equations is expressed in the generalized coordinate system, with: $\mathcal{s}_1 = 0.00148$, $\mathcal{s}_2 = 0.6331$, $\mathcal{s}_3 = -0.63269$, $m_1 = 0.0000303$, $m_2 = 0.0000362$ and $m_3 = 0.0000000178$.

Finally, Table 2 shows the comparison between ANSYS and CMT values, evidencing an average error of 4.15% in the first six modes of vibration. It is important to note that the CMT result was weighted in Table 2 by an adjustment factor of 2/3, for the 1st and 4th mode of vibration, in addition to the more complex adjustment coefficient for the 5th and 6th modes, in the value of 1/1.3, which can be explained by Dziewolski [4] and Melo [16]. The weighting by $k_{aj} = \frac{1}{2}$ for the 2nd and 3rd is also verified, serving as an extrapolation of that postulated in [4, 16]. Finally, it should be noted that the adjustment coefficients in the 5th and 6th modes are due to a peculiarity in the operation of Flexion-Torsion when only the torsion is generated by the deformation modes, which are exposed in the modeling of ANSYS by Def. [14] and [18], as shown in Figure 11i and Figure 12.

Table 2: Comparative result of the six first modes of vibration for the reinforced concrete column, in application 1, computing: $\Delta(\%) = \frac{|f_{ANSYS} - f_{TMC}^*|}{f_{TMC}^*} \cdot 100$

Modes of vibration	*Deformation in ANSYS*	f_{TMC} (Hz)	Adjustment coefficient k_{aj}	$f_{TMC}^* = k_{aj} \cdot f_{TMC}$ (Hz)	f_{ANSYS} (Hz)	Δ(%)
1º	Def. [5]	0.49174	2/3	0.32783	0.32192	1.80
2º	Def. [29]	3.68446	1/2	1.84223	1.90040	3.16
3º	Def. [25]	10.14482	1/2	5.07241	5.00040	1.41
4º	Def. [12]	13.47404	2/3	8.98269	8.80310	2.00
5º	Def. [19]	16.18048	1/1.3	12.44652	13.75100	10.48
6º	Def. [1]	21.68748	1/1.3	16.68268	17.69200	6.05
				Average error in the six first Modes of Vibration		4.15
				Average error in the three first Modes of Vibration		2.12

This is for coefficient $\lambda = H \cdot \sqrt{\mathcal{s}_1} \equiv 100\ \text{m} \cdot \sqrt{0.00148} = 3.84$, where it is obtained through the decoupling flowchart presented in Figure 10. Then, Table 2 is used with proper frequency values, in light of the calculated coefficient λ, as postulated in Table 3.

Table 3: Frequency and period of the six first Modes of vibration for the thin-walled column, for use in application 1, with coefficient $\lambda = 3.84$

λ	Mode	$i = 1$	$i = 2$	$i = 3$	$i = 4$	$i = 5$	$i = 6$
3.84	λ_1	2.35747	5.01494	8.10498	9.30600	10.17856	11.75585
	λ_4	1.31060	4.61623	7.86452	9.09734	9.98815	11.59138
	ω_i^*	3.08969	23.15014	63.74179	84.65987	101.66494	136.26648
	f_i^*	0.49174	3.68446	10.14482	13.47404	16.18048	21.68748

According to the procedures described, a result very close to the same example modeled via MEF in ANSYS was obtained with an average approximation of 95.85 % in the first six modes of vibration for activation of the lintels as a bar, as shown in Figure 11 by the value of the simulation in ANSYS.

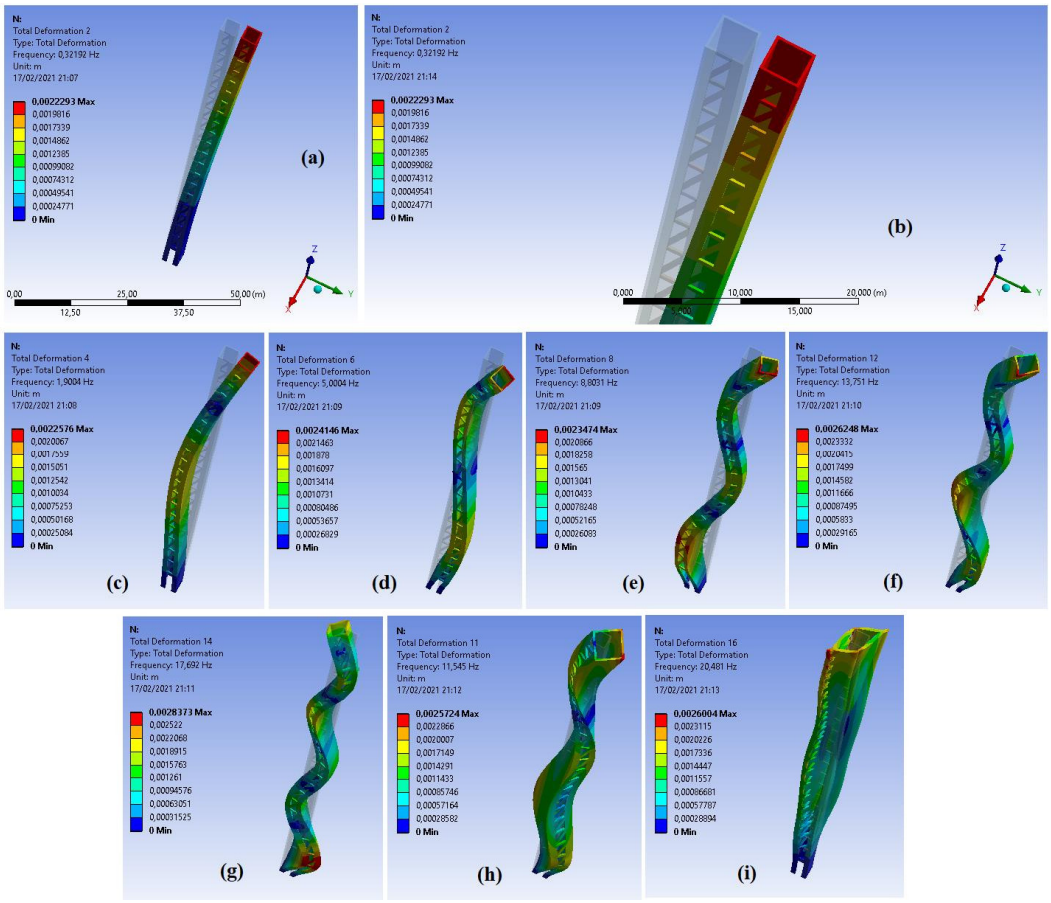

Figure 11: Results of the frequencies of the concrete Structural core with Z lintels in ANSYS: (a) 1st mode of vibration, (b) details of the deformation by flexion of the lintels in the 1st mode of vibration, (c) 2nd mode, (d) 3rd mode, (e) 4th mode, (f) 5th mode, (g) 6th mode, (h) mode of deformation [18] characterized by torsion and (i) mode of deformation [14] characterized by torsion

Finally, Figure 12 shows the frequency convergence curve of the 1st mode of vibration with the mobilization of the lintels under flexion, thus demonstrating that the analyzed frequency values match with precise values.

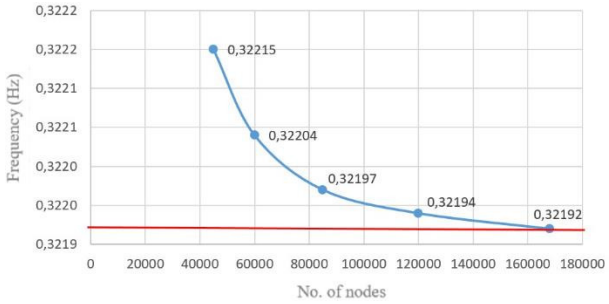

Figure 12: Convergence curve of the frequency of the 1st Mode of vibration of the column, based on the number of nodes in the finite elements, for the Z-Bracing

7.2 Aplication 2

In this second application, the thin-walled column is modeled in C-core with a height of $H = 100\ m$, and braced by lintels arranged in X. And to this end, via CMT/WPT, the structural

scheme arranged in Figure 7a and Figure 9a is followed, where the dimensions of the structural elements are: $b_1 = b_2 = b_3 = 3.45$ m and $b_4 = b_5 = 1.00$ m for the Wall Panels with thickness $t = 0.25$ m and molded with reinforced concrete of characteristic compression resistance: $f_{ck} = 50$ MPa, in addition to lintels with the following dimensions and arrangements: $\ell = 1.45$ m, $e_a = e_d = 0.25$ m, $h_i = h_f = 1.15$ m, $d_i = d_f = 0.50$ m, $d_i^* = d_f^* = 0.62$ m, $h_a = h_d = 0.5$ m, $\gamma_a = 63^{\circ}$, $\gamma_d = 297^{\circ}$ and $\ell_a = \ell_d = 1.092$ m. According to the load acting on the column, as shown in Figure 9b, under the distribution: $q_1 = 50\,\frac{\text{kN}}{\text{m}}$, $q_2 = 0\,\frac{\text{kN}}{\text{m}}$ and $Q = 0$ kN, the system of differential equations of the dynamic analysis is expressed, according to Eq. (19), modifying only the values of the elements of the stiffness matrix $[S]$ of the X-Bracing system, where: $S_a = -2.808 \cdot 10^4$, $S_b = -1.397 \cdot 10^{-9}$ and $S_c = 1.115 \cdot 10^6$. After the diagonalization of the EDPs system of the dynamic analysis of the X braced WPT, according to the flowchart provided in Figure 10, the diagonalized matrix $[\mathcal{s}]$ is obtained, expressed by:

$$[\mathcal{s}] = \begin{bmatrix} 0.002121 & 0 & 0 \\ 0 & 0.63336 & 0 \\ 0 & 0 & -0.63265 \end{bmatrix} \tag{20}$$

The modes of vibration via CMT are calculated through Table 4, with the coefficient $\lambda = H \cdot \sqrt{\mathcal{s}_{11}} = 100\text{ m} \cdot \sqrt{0.002121} = 4.60$. Table 5 contains the comparison between the frequencies of the first six modes of vibration, via CMT and ANSYS, with an error of 5.29 % for the first three modes of vibration.

Table 4: Frequency and period of the six first Modes of vibration, for use in application 2, with $\lambda = 4.60$

$\boldsymbol{\lambda}$	Mode	$\boldsymbol{i = 1}$	$\boldsymbol{i = 2}$	$\boldsymbol{i = 3}$	$\boldsymbol{i = 4}$	$\boldsymbol{i = 5}$	$\boldsymbol{i = 6}$
4.60	λ_1	2.69791	5.07267	8.14539	9.34825	10.20977	11.76949
	ω_i^*	4.41567	23.31883	64.00607	85.05869	101.91345	136.20148
	f_i^*	0.70278	3.71131	10.18688	13.53751	16.22003	21.67714

Table 5: Comparative result of the six first Modes of vibration in application 2

Modes of vibration	*Deformation in ANSYS*	$\boldsymbol{f_{TMC}}$ (Hz)	Adjustment coefficient $\boldsymbol{k_{aj}}$	$\boldsymbol{f_{TMC}^* = k_{aj} \cdot f_{TMC}}$ (Hz)	$\boldsymbol{f_{ANSYS}}$ (Hz)	Δ(%)
1º	Def. [5]	0.49174	1/2	0.35139	0.32032	8.84
2º	Def. [29]	3.68446	1/2	1.85566	1.93350	4.20
3º	Def. [24]	10.14482	1/2	5.09344	5.23740	2.82
4º	Def. [12]	13.47404	2/3	9.02501	9.35760	3.69
5º	Def. [19]	16.18048	1/1.3	12.47695	15.16000	21.51
6º	Def. [1]	21.68748	1/1.3	16.67472	19.56800	17.35
				Average error in the six first Modes of Vibration		9.74
				Average error in the three first Modes of Vibration		5.29

In addition to evidencing a convergence of 90.26 % for the CMT in the first six modes of vibration, based on Figure 13, highlighting the presence of the adjustment coefficients $k_{aj} = \frac{1}{2}$ for the 2nd and 3rd modes of vibration. Thus, the simple operation is configured, which adjustment factor of 2/3 to the 1st mode, for the operation even simpler than the previous one,

using the one recommended in [4]. In the 5th and 6th modes of vibration, the adjustment is made using $k_{aj} = \frac{1}{1{,}3}$, configuring the complex operation. This is due to the peculiarity generated by the torsional deformation modes, see Figure 14a and Figure 14b. And finally, the convergence curve of the 1st mode of vibration with the X lintels is shown in Figure 14c, being this a structural mode of operation of the lintels as bars under flexion.

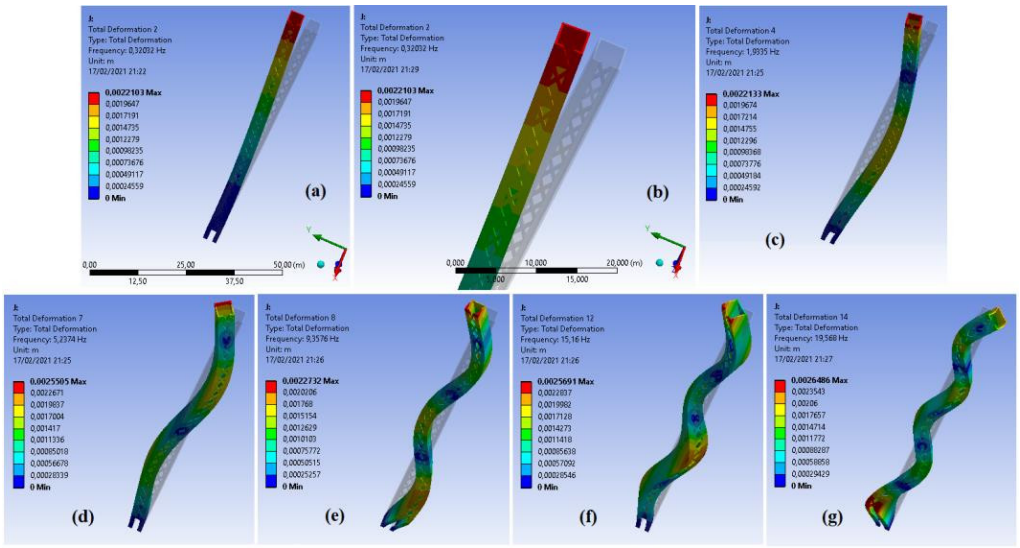

Figure 13: Results of the frequencies of the concrete Structural Core with X lintels in ANSYS: (a) 1st mode of vibration, (b) details of the deformation by flexion of the lintels in the 1st mode of vibration, (c) 2nd mode, (d) 3rd mode, (e) 4th mode, (f) 5th mode, and (g) 6th mode

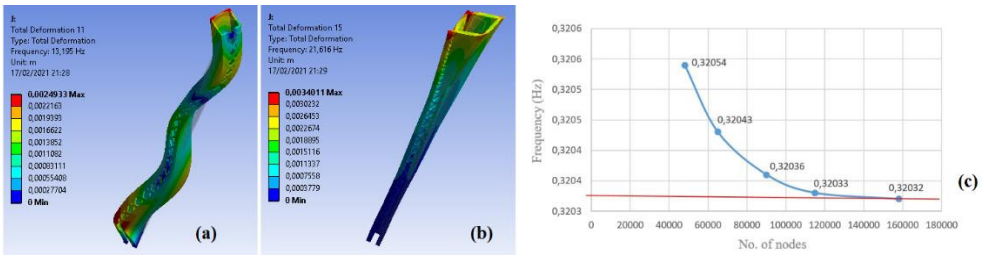

Figure 14: Results of the frequencies of the concrete Structural Core with X lintels in ANSYS: (a) mode of deformation [18] characterized by torsion, (b) mode of deformation [8] characterized by torsion and (c) convergence curve of the frequency of the 1st mode of vibration of the column, based on the number of nodes in the FEM, for the X-Bracing

8 CONCLUSIONS

The great contribution of this article is the postulation of the routine of easy manipulation to quantify the first modes of vibration, being applicable for thin-walled columns in the shape of a C-core and braced by lintels in Z and X on the open face. Thus, structural engineers are able to analyze the frequency values for modeling carried out with commercial software, thus seeking to move the frequency of the forces $\overline{\omega}$ away from the natural frequencies ω of vibration of the structure, preventing the amplification of deformations. In addition, with such formulation, designers can perform preliminary studies to detect the best diagonal slope of the lintels, generating rationality to the structural design of C-core columns. The complete equation of the bracing system in Z and X is proceeded as an innovation, using Maney's equations to

model the bar finite element relevant to the horizontal and diagonal lintels, and increasing in the lintel modeling the Matrix Analysis to consider, in this way, the incidence of the referred lintels. Then, Matrix Condensation is used in order to express all the results only at the points of convergence, O_i and O_f, defined on the axis of the Wall Panels (4) and (5).

Then, the bar finite element of the lintels is converted into Elastic Reactions distributed in the Continuous Medium, thus promoting the interconnection in the modeling of the lintels with the Continuous Medium Technique employed in the thin-walled column. In concomitance with the aforementioned conversion, the adaptation of the Wall Panel Theory to accommodate the axial Elastic Reactions of the lintels, as well as their degrees of freedom, is performed. And finally, the Modal Analysis of the aforementioned column and bracing system is structured, linking the Structure Dynamics applied to the Continuous Medium to the modeling of the Wall Panels.

It is important to point out that in the validation of the Z and X-Bracing formulations, operationalized via CMT, particular cases of the C-section that appear in the literature were used, improving two new bracing models, which are the proposition of this article. It is noteworthy that the numerical examples were simulated with ANSYS to promote the validation of the proposed formulation via CMT, observing the best distribution of the finite elements in the software, in addition to having the theoretical care in refining the finite element mesh. Finally, an approximation of 90.26 % was found for the first six Modes of vibration for the column shaped in structural C-core and X-braced. As for the case of Z-Bracing, there was a discrepancy of only 2.12% between the CMT frequency values and modeling with ANSYS. This is for the first three modes of vibration, which represent the largest amplitudes and relevance to the correct and safe structural dimensioning.

REFERENCES

[1] A. Carpinteri, G. Lacidogna and G. Nitti. Open and closed shear-walls in high-rise structural systems: static and dynamic analysis. *Curved and Layer. Struct*, 3(1):154–171, 2016. https://doi.org/10.1515/cls-2016-0013.

[2] L. Chitty. On the cantilever composed of a number of parallel beams interconnected by cross bars. *Philosophical Magazine and Journal of Science*, 38:685–699, 1947. https://doi.org/10.1080/14786444708521646.

[3] C. A. O. Donneys. *Análise de estruturas de edifício alto submetidas a carregamento sísmico pela técnica do meio contínuo*. Master thesis, Escola de Engenharia da Universidade de São Paulo, São Carlos, SP, Brasil, 2015. Disponível em <https://teses.usp.br/teses/disponiveis/18/18134/tde-02032016-105216/publico/2015ME_CarlosAndresOrozcoDonneyscomfolhadejulgamento.pdf>.

[4] R. Dziewolski. Étude théorique et expérimentale d'une poutre em caisson asymétrique avec deux apêndices. *IABSE congresso report*, 131–137, 1964.

[5] J. E. Goldberg. Wind stresses by Slope Deflection and converging approximations. *Transactions of the American Society of Civil Engineers*, 99:962–984, 1934. https://doi.org/10.1061/TACEAT.0004526.

[6] M. Hoit. *Computer-Assisted Structural Analysis and Modeling*. Prentice Hall, 1995.

[7] A. Kheyroddin, D. Abdollahzadeh and M. Mastali. Improvement of open and semi-open core wall system in tall buildings by closing of the core section in the last story. *Internation Journal Advanced Structures Engineering*, 67(6):1–12, 2014. https://doi.org/10.1007/s40091-014-0067-0.

[8] J. S. Kuang and S. C. Ng. Coupled vibration of tall building structures. *The Structural design of Tall and Special Buildings*, 13:291–303, 2004, https://doi.org/10.1002/tal.253.

[9] M. Laredo. *Grands Batiments: Contreventements, Dynamique des Structures & Calcul Automatique*. Éditions Eyrolles, 1977.

[10] G-Q. Li, M-D. Pang, Y-W. Li, L-L. Li, F-F. Sun and J-Y. Sun. Experimental comparative study of coupled shear wall systems with steel and reinforced concrete link beams. *Structural design of Tall and Special Buildings*, 28(18):1–17. 2019, https://doi.org/10.1002/tal.1678.

[11] I. A. MacLeod. Lateral stiffness of shear walls with openings. *Tall Buildings: The Proceedings of a Symposium*, 223–244, 1967. https://doi.org/10.1061/(ASCE)0733-9445(2006)132:11(1846).

[12] E. Mancini and W. Savassi. Tall building structures unified plane panels behaviour. *The Structural Design of Tall Buildings*, 8:155–170, 1999. https://doi.org/10.1002/(SICI)1099-1794(199906)8:2%3C155::AID-TAL125%3E3.0.CO;2-6.

[13] G. A. Maney. Secondary stresses and other problems in rigid frames: a new method of solution, *Studies in Engineering*, 1:1–17, 1915.

[14] S. A. Meftah and A. Tounsi. Vibration characteristics of tall buildings braced by shear walls and thin-walled open-section structures. *The Structural design of Tall and Special Buildings*, 17:203–216, 2008. https://doi.org/10.1002/tal.346.

[15] T. H. G. Megson. *Structural and Stress Analysis*. Elsevier, 2005.

[16] W. I. G. Melo. Contribuições à análise dinâmica da ação do vento em Pilares de Pontes via Técnica do Meio Contínuo e Método dos Elementos Finitos. PhD thesis, UFPB, Universidade Fedral da Paraíba, João Pessoa, PB, Brasil, 2019. Disponível em <https://sig-arq.ufpb.br/arquivos/20200630605626186276475430448 7c5b/2019DO_WeslleyGomes_PDF_DEFINITIVO.pdf >.

[17] W. I. G. Melo and N. P. Barbosa. Dynamic Modeling of Metal Columns with Open Thin-Walled Sections. *International Journal of Steel Structures*, 20(3):833–855, 2020. https://doi.org/10.1007/s13296-020-00326-4.

[18] W. I. G. Melo and N. P. Barbosa. Dynamic decoupling in reinforced concrete columns in structural core shape and applied to bridges. *International Journal of Advanced Engineering Research and Science*, 7(5):48–58, 2020. https://doi.org/10.0.86.145/ijaers.75.7.

[19] W. I. G. Melo and N. P. Barbosa. Pilares de Pontes com seção de paredes finas e elevada altura, uma análise teórica e numérica pela Técnica do Meio Contínuo e pelo Método dos Elementos Finitos. *Revista de Engenharia da Universidade Católica de Petrópolis*, 14(1):25–45, 2020. Disponível em: <http://seer.ucp.br/seer/index.php/REVCEC/article/view/1840>.

[20] S. C. Ng and J. S. Kuang. Coupled vibration of structural thin-walled cores. *Acta Mechanica Solida Sinica*, 13(1):81–88, 2000.

[21] A. Pluzsik and L. P. Kollár. Effects of shear deformation and restrained warping on the displacements of composite beams. *Journal of Reinforced Plastics and Composites*, 21(17):1517–1541, 2002. https://doi.org/10.1177/0731684402021017927.

[22] G. Potzta and L. G. Kollár. Analysis of building structures by replacement sandwich beams. *International Journal of Solids and Structures*, 40:535–553, 2003. https://doi.org/10.1016/S0020-7683(02)00622-4.

[23] A. M. Quarteroni, R. Sacco and F. Saleri. *Méthodes numérique: algorithms, analyse et applications*. Springer, 2007.

[24] J. Ricaldoni. *Nota sobre el Efecto de Torsion em Edificios Elevados*. Publicaciones del Instituto de Estática, Nº 16, 1958.

[25] J. Ricaldoni. *Curso de estructuras metálicas: Naves Metalicas*. Publicaciones del Instituto de Estática, Nº 19, Tomo II, 1, 1961.

[26] R. Rosman. Dynamics and stability of shear wall building structures. *Proceedings of the Institution of Civil Engineers*, 55(2):411–423, 1973. https://doi.org/10.1680/iicep.1973.4875.

[27] W. Schueller. *The Vertical Building Structure*. Van Nostrand Reinhold, 1990.

[28] L. Szerémi. Stiffening system of multi-storey buildings by the continuum model. *Periodic Civil Politechnica*, 22:205–218, 1977.

[29] G. Varjú and A. Prokié. The influence of lintel beams and floor slabs on natural frequencies of the tall buildings core – numerical and experimental studies. *Periodica Polytechnica Civil Engineering*, 59(4):511–520, 2015. https://doi.org/10.3311/PPci.8410.

[30] B. Z. Vlassov. *Pièces longues em voiles minces*. Éditions Eyrolles, 1962.

[31] E. Volterra and E. C. Zachmanoglou, *Dynamics of Vibrations*. Editions by Charles E. Merrill, 1965.